Tuning Transition Metal Carbides Activity by Surface Metal Alloying: Case Study on CO_2 Capture and Activation

Martí López,[†] Luke Broderick,[‡] John J. Carey,[‡] Francesc Viñes,[†,*] Michael Nolan,[‡,*] and Francesc Illas[†]

[†] *Departament de Ciència de Materials i Química Fisica & Institut de Química Teòrica i Computacional (IQTCUB), Universitat de Barcelona, Martí i Franqués 1-11, 08028 Barcelona, Spain*

[‡] *Tyndall National Institute, Lee Maltings, University College Cork, Cork T12R5CP, Ireland.*

ABSTRACT

CO_2 is one of the main actors in the greenhouse effect and its removal from the atmosphere is becoming an urgent need. Thus, CO_2 capture and storage (CCS) and CO_2 capture and usage (CCU) technologies are intensively investigated as technologies to decrease the concentration of atmospheric CO_2. Both CCS and CCU require appropriate materials to adsorb/release and adsorb/activate CO_2, respectively. Recently, it has been theoretically and experimentally shown that transition metal carbides (TMC) are able to capture, store, and activate CO_2. To further improve the adsorption capacity of these materials, a deep understanding of the atomic level processes involved is essential. In the present work, we theoretically investigate the possible effects of surface metal doping of these TMCs by taking TiC as a textbook case and Cr, Hf, Mo, Nb, Ta, V, W, and Zr as dopants. Using periodic slab models with large supercells and state-of-the-art density functional theory based calculations we show that CO_2 adsorption is enhanced by doping with metals down a group but worsened along the *d* series. Adsorption sites, dispersion and coverage appear to play a minor, secondary constant effect. The dopant-induced adsorption enhancement is highly biased by the charge rearrangement at the surface. In all cases, CO_2 activation is found but doping can shift the desorption temperature by up to 135 K.

* Corresponding authors: francesc.vines@ub.edu, michael.nolan@tyndall.ie

1. INTRODUCTION

Every year increasing evidence of the significant impact of global warming on Earth are being reported.[1,2] The environmental prediction models show a non-optimistic future if no urgent measures are taken to face this issue.[3,4] Atmospheric CO_2 is one of the greenhouse gases with highest impact, and its environmental effects are particularly problematic. Apart from well-known ones such as ocean acidification,[5] there are predictions that while the anthropogenic emissions CO_2 rise into the atmosphere, the CO_2 concentration and the concomitant global warming will rise exponentially through carbon-cycle feedbacks.[4] Despite worldwide efforts in controlling and reducing CO_2 emissions, as exemplified in active environmental protocols such as Copenhagen, Kyoto, or Paris,[6-8] recently the International Energy Agency (IEA), in its global energy and CO_2 status reports, announced an increase of 1.4% in energy-related CO_2 emissions.[9]

Among many strategies oriented at reducing CO_2 emissions or at decreasing its atmospheric concentration, an appealing one is the removal of atmospheric CO_2 *via* scrubber materials.[10,11] Spurred on by the urgent requirements of the Paris protocol, CO_2 surface chemistry[12] is experiencing a renewed interest focusing on characterizing scrubber materials and to optimize their properties in CO_2 capture and storage (CCS).[13,14] Along this line, a desirable advance is not only in CO_2 capture, but its chemical activation and eventually re-use as a carbon feedstock to synthesize other valuable chemicals through the commonly known CO_2 capture and usage (CCU) strategies.[15] Given the high CO_2 chemical stability, only a few *privileged* materials are able to selectively adsorb CO_2 strong enough for CCS or CCU technologies. Moderate to high CO_2 adsorption energies usually indicate an activation of the molecule,[12] which often occurs through a charge transfer from the surface of a material to the CO_2 $6a_1$ anti-bonding molecular orbital, thus weakening the C-O bonds and leading to a bent geometry.[10] From this point on the $CO_2^{\delta-}$ molecule is much more reactive than the neutral one and the starting point for any industrial process to reuse CO_2.

From all known possible materials, transition metal carbides (TMC) have shown promising results in the CO_2 capture, storage, and activation,[10,16,17] even conversion to valuable chemicals[18] while their relatively low cost makes them industrially attractive materials. Diverse density functional theory (DFT) based computational studies, mostly focused on early TMCs, proved that these materials display significant potential for CO_2 activation.[19,20] In particular, TiC, WC, and especially α-Mo_2C excel among the family of TMCs, and so, have been studied in deeper detail. These TMCs have proven their CCS potential but also their CCU capabilities, as highlighted by their CO_2 based catalytic activity,[17,18] including CO_2 hydrogenation towards

methanol.[21] Additional systematic DFT based studies report a strong CO_2 adsorption on most stable (001) surface of rocksalt crystal group IV (TiC, ZrC, WC), group V (NbC, TaC), and group VI (δ-MoC) TMCs with a concomitant activation of the adsorbed molecule,[10] indicating that these materials may be adequate for CCU technologies.

In the search for tailor-made materials for CCS and/or CCU, different ways of tuning the surface activity towards CO_2 can be envisaged, including the use of surface doping agents. This is a common practice when considering metal and metal oxide properties, thus locally tuning the chemical activity or stabilizing certain facets as in F-doped TiO_2 nanoparticles.[22,23] It has also been shown that the presence of surface dopants promotes the oxygen vacancy formation on CeO_2 nanoparticles.[24,25] Also, CO adsorption on ceria is easily enhanced by adding Zr or Ti on the bulk, improving CO oxidation and releasing CO_2 to the atmosphere.[26] In the case of metals, metal alloying is a standard, but not yet fully understood or controlled, approach to modulate the surface activity. Bimetallic TMCs using earth-abundant and cheap metals, such as Fe_3Mo_3C or Ni_6Mo_6C, have been previously prepared, *via* stepwise reduction of precursor oxides,[27] opening the path towards an economically reasonable synthesis procedure. Moreover, there have been clear improvements in the understanding of nanoalloys,[28] thus opening the door to future control.

In the present work we explore transition metal doping —or surface metal alloying— on TMCs surfaces in the context of CO_2 capture, storage, and activation. Here, TiC has been chosen to understand how the CO_2 adsorption energy is affected by the presence of a surface or subsurface doping agent. The dopants scrutinized are Zr, Hf, V, Nb, Mo, Cr, Ta, and W; a subset of transition metals that are known to form metal carbides. This work therefore aims to assess the significant possibility of bimetallic/doped TMCs for use in CCS and the implications for design of materials with enhanced CO_2 adsorption, following a kinetic rate balance approach successfully used in previous works of some of the authors concerning CO_2 adsorption on TMCs.[10] Furthermore, the CO_2 anchoring and activation is regarded a first, necessary, and determining step for CO_2 conversion through CCU applications.

2. SURFACE MODELS AND COMPUTATIONAL DETAILS

Calculations reported in the present work have been carried out within the density functional theory (DFT),[29,30] using the Perdew, Burke, and Ernzerhof (PBE) implementation of the generalized gradient approximation (GGA) of the exchange-correlation functional[31] as implemented in the Vienna *Ab Initio* Simulation Package (VASP).[32-34] The electronic density of the valence electrons has been expanded using a plane-wave basis set with an energy cut off

450 eV. The interactions between the core and valence electrons have been taken into account through the projector augmented wave (PAW) approach of Blöchl,[35] as implemented by Kresse and Joubert.[36] The atomic relaxation optimization has been carried out until forces acting on atoms were less than 0.02 eV $Å^{-1}$, and the electronic energy convergence is set to 10^{-5} eV. The convergence of the calculations has been enhanced using a Gaussian smearing method with a smearing width of 0.2 eV, yet final energies are taken extrapolated to 0 K (no smearing). The calculations are non spin-polarized. Calculations incorporating spin polarization have been performed for the pristine and doped surfaces, where the doping metal can show different spin configurations, *e.g.*, for Cr case, although no solutions were found with an excess of one spin, i.e. magnetic minima and the effect of spin polarization on relative energies is negligible. Monkhorst Pack **k**-points sampling grid[37] of (2×2×1) **k**-points has been used to carry out the necessary numerical integration in the reciprocal space.

A $(2\sqrt{2}\times2\sqrt{2})R45^{o}$ supercell slab model has been used to represent the TiC (001) surface. The model consists of six stoichiometric atomic layers extended in the *xy* plane, containing eight C and Ti atoms per layer, with a vacuum gap of 15 Å in the *z* direction. The CO_2 molecules have been introduced 2 Å far away from the surface along the *z* direction and different initial adsorption sites and orientations relative to the surface have been systematically sampled. The two bottom layers of the slab are fixed to simulate the bulk structure of the materials. The dopants have been placed on the surface of TiC substituting a Ti ion and considering several situations regarding the adsorbed CO_2 molecule. Given the lack of work on doped metal carbides to date, we have used a doping concentration of 3.125%, which is typical for doping concentrations in, *e.g.* metal oxides. All ionic relaxations were carried out using the TiC bulk optimized slab geometry. A check on the effect of further optimization of the slabs in the slab plane in which doping atoms are included results in a negligible change to the CO_2 adsorption energies which is no larger than 0.04 eV. The necessary calculations for the isolated, gas phase, CO_2 molecule as well as for the isolated metal atoms, have been carried out in an asymmetric box of (9×10×11) Å to force molecular orbital correct occupations. In the case of isolated metal atoms, spin-polarized calculations have been carried out to correctly describe their open shell nature.

3. RESULTS AND DISCUSSION

3.1. Dopant effects on the TiC surface

The substitution of Ti atom of the TiC(001) surface, either at the surface of subsurface atomic layers, by one atom of Cr, Hf, Mo, Nb, Ta, V, W, or Zr as a dopant has two main effects; namely

surface geometry and charge density distortions. These changes come from the difference of atomic radii and electronic configuration of the transition metal dopants relative to Ti.

For all investigated cases, the dopant at the surface site was energetically preferred over the subsurface one; difference in energies of both situations, $\Delta E_{sub\text{-}surf}$, are reported in Table 1, with generally a strong preference for dopants to be at the surface by in between circa 0.35 and 0.65 eV with exceptions for V and Ta. Given the commented different radii between Ti and dopant atoms, one would think that the latter can be better embedded at the surface sites than at the subsurface ones simply because lattice distortions are minimized when the dopant occupies a surface site, i.e., they are better accommodated. From this reasoning one would also expect that as closer the dopant is to Ti in the periodic table, smaller the energetic difference between surface and subsurface positions would be, which is indeed confirmed by the calculations reported in Table 1. The preference for substitution at surface sites may be beneficial for catalytic purposes when this situation is accompanied by a sought for chemical activity. This fact suggests that control of the TMCs surface chemistry is therefore possible.

A further point to be considered is the energy cost for cation exchange, here denoted as ΔE_{dop}. Table 1 reports these energies, taking isolated atoms in vacuum as the reference, where negative energies indicate stability, and reveals that not all substitutions are energetically favorable. The doping by the same group IV Zr and Hf is thermodynamically driven. Along group V (Ta, Nb, and V), doping is also thermodynamically feasible, yet gradually the stability decreases by going down a group. Finally, in group VI only Mo is energetically driven whereas Cr and W, which do not feature a rocksalt carbide, show unfavorable (positive) exchange doping energies. Thus, apparently, the ability of the TM dopant to crystallize in a rocksalt environment appears to be a determining factor.

Focusing deeper on the structural aspects, see Table 1, charge density distortions caused by the dopant are present in the neighboring C atoms only, which means that the doping clearly has a local effect. This is also observed when inspecting changes in the electron density affecting both the dopant agent and the surrounding C atoms. For instance, in the pristine TiC (001) surface, the Bader analysis[38] for the C atoms in the outermost atomic layer predicts a charge of -1.70 *e*; a slightly larger value of -1.74 *e* is found for the C atoms in the second layer, Dopants with an oxidation state higher than Ti (+1.74 *e*), such as the extreme case of Hf, which as a surface dopant exhibits a Bader charge of +2.03 *e*, spread this charge excess over with directly bonded C atoms; there are four at the surface layer with a charge of -1.74 *e*, and one subsurface C with a charge of -1.90 *e*. At the other extreme, Cr, with a charge of +1.31 *e*, implies a lower charge transfer, and, consequently, the neighboring C atoms are less negatively charged, with computed Bader charges of -1.58 *e* for surface carbon and -1.64 *e* for subsurface carbon.

A complete set of calculated Bader charges for the different situations explored in the present work may be found in Table S1 of the Supporting Information.

3.2. Binding modes of CO_2 on doped TiC (001)

A previous thorough study explored several binding modes of CO_2 on a set of TMC (001) surfaces and considered situations in which the molecular axis lies perpendicular or parallel to the carbide surface.[10] Approaching the CO_2 molecule to the surface in a perpendicular orientation, *i.e.* anchoring by one of its O atoms, results in no clear chemisorption. On the other hand, the approach of the CO_2 molecule with its molecular axis parallel to the surface leads to chemisorbed states, which then often lead to an activated, adsorbed, bent adsorption species. In this case, two main competitive adsorption configurations are found, both implying a bond between the CO_2 molecule and a surface C atom and with the O atoms nearly above the surface metal atoms. These two bonding models are the so-called TopC and MMC, see Figure 1. However, in the presence of a doping metal, the TopC situation presents two possible conformations; TopC and TopC-adjacent depending on the relative orientation of the plane formed by the atoms of the activated CO_2 molecule relative to the plane formed by the dopant atom, the surface C atom, and the C atom of the CO_2 molecule (Figure 1). The difference here is that in TopC adjacent the CO_2 molecule does not have any direct interactions with the dopant site. In pristine TiC, both modes present similar binding energies (Table S2, within the accuracy of the PBE calculations) having both modes a competitive interaction, but since MMC mode was never preferred for any doped system, TopC was used for the oncoming detailed exploration of the doped systems.[10]

3.3. CO_2 adsorption strength

The CO_2 adsorption energy, E_{ads}, on the pristine or doped TiC(001) surface, is obtained as in Eq. (1)

$$E_{ads} = E_{Sur-CO_2} - (E_{CO_2} + E_{Sur}) \quad (1),$$

where E_{Sur-CO_2} is the energy of the surface with adsorbed CO_2, E_{Sur} the energy of the clean pristine or doped TiC surface, and E_{CO_2} the energy of the gas phase molecule, respectively. Within this definition, the more negative the E_{ads}, the stronger the adsorption. From all the set of investigated dopants, the case with Hf located in the first atomic layer exhibits the largest adsorption energy (-0.96 eV for TopC). This is interpreted in term of the larger positive charge

on Hf compared to Ti (see Table S1), which induces a stronger stabilization through a coulombic Hf-O interaction as clearly seen in Figure 2. This implies that the adsorption energies involving early TMs as dopants are larger than those involving late TMs (Table 2), with one of the weakest situations being W (-0.22 eV). However, the case of Ta represents an exception to this rule since even with a quite a large charge of +1.91 e, it displays a slightly smaller E_{ads} (-0.57 eV) than pristine TiC. In any case, it is clear that the dopant charge is a determining factor although not the only one.

Concerning doping with W, the TopC adjacent situation implies a slightly higher adsorption energy (-0.31 eV), but this is still far from the -0.61 eV for undoped TiC. Hence, the doping effect has still a vicinal, in this case worsening, effect. The opposite applies to Hf, where TopC adjacent leads to a reduced adsorption energy of -0.81 eV. These two limiting situations (Hf and W) are selected to study the effect of dispersion and also of proximity of the dopant to the adsorption site.

Dispersion effects are evaluated for all the examples of CO_2 adsorption that we have studied (see Table S2), using the Grimme D3 correction,[39] as earlier studied for CO_2 adsorption on TMCs.[10] As expected, the adsorption energies increase (in absolute terms) by -0.24 up to -0.29 eV, but, more importantly, variations in this shift among the dopants are no larger than 0.05 eV. The only exception is CO_2 adsorption in MMC mode on Cr-TiC where such energy difference is -0.32 eV. Consequently, the effect of van der Waals type forces on the doping increase/decrease of the CO_2 adsorption energies can be considered a constant shift and can be safely disregarded in the oncoming discussion.

In a similar fashion, the dopant effect has been tested where the dopant is positioned farther from the CO_2 than in the TopC-adjacent situation. To this end, a larger $(3\sqrt{2}\times3\sqrt{2})R45^{o}$ supercell is used, see Figure S1. There, because of the different number of plane waves associated to the cell dimensions and the concomitant different density of **k**-points, the CO_2 adsorption energy on undoped TiC(001) is -0.51 eV. When the CO_2 is placed on the TopC situation close to Hf, computed adsorption energy strengthens to -0.89 eV, in line with results above discussed. However, when the CO_2 is placed farther away from the Hf atom, the E_{ads} becomes -0.52 eV, which is very close to that of pristine non-doped TiC. This is another clear evidence of the very local nature of the dopant effect in the carbide-CO_2 interactions.

This finding can be further supported by calculations for the W doped surface with TopC E_{ads} of -0.14 eV but -0.49 eV when CO_2 is on a TopC site farther away from W, thus showing a difference of only 0.02 eV from the result for undoped TiC. In line with the above-commented charge density distortions (see also Table S1), we consider in the following that the doping

effect is completely local and focus on the situations where CO_2 is close to the doping atom as in Figure 1.

Finally, the same two doping agents (Hf and W) have been used to evaluate possible effects due to dopant saturation/coverage on the surface. To this end, an extra CO_2 with its correspondent dopant have been added to the $(2\sqrt{2}\times2\sqrt{2})R45^{o}$ unit cell, effectively increasing the doping concentration and also the CO_2 coverage (see Figure S2). The results, as expected, reveal a reduction of the mean adsorption energies to -0.77 eV for the case of Hf and -0.13 eV for that of W. Interestingly, the local nature of the dopant effect prevails, a strengthening of the interaction is observed for Hf, and a weakening for W. The reduction with respect to the low coverage case is mostly due to steric repulsion between adsorbates.

3.4. Activated CO_2 structure

In all cases where the surface-CO_2 interaction leads to a C-C type of bond, similar structural changes appear for the adsorbed CO_2 molecule. The O-C-O angle is reduced from 180^{o} to < 130^{o} and the C-O distances are elongated with bond lengths in the 1.28-1.30 Å range, thus larger than the computed PBE value of 1.16 Å for CO_2 in vacuum (Table S3). For the studied TopC cases, where a clear interaction exists between one of the O atoms of the CO_2 molecule and the dopant, the symmetry of the CO_2 bonds is slightly broken with the C-O distances featuring differences of up to 0.02 Å. One can speculate that this lack of symmetry might have an impact in the subsequent CO_2 usage since one of the C-O bonds appears to be more activated with a preference for further reactions as the CO_2 dissociation upon hydrogenation.[10]

3.5. Charge transfer

Additional information to better understand the observed trends in CO_2 adsorption energy triggered by the presence of the dopant is gained by analyzing the net charges on relevant atoms as obtained from the Bader's *atoms-in-molecules* analysis of the total electron density.[38] To this end two possibilities are investigated involving the relationship between E_{ads} and the initial Bader charges of the doped surface (Table S1), or with the net charge transfer from the doped-surface to CO_2 (Table S3). The first relationship, summarized in Figure 3, strongly supports that the more oxidized the dopant, then the stronger is the adsorption of CO_2. This is in agreement with the previously discussed charge modifications on the surface electronic structure due to the presence of the dopant.

The chemistry behind this trend is quite simple. A more oxidized cation leads to higher negative charge in the neighboring C atoms (Table S1) directly interacting with the adsorbate;

this is a feature that favors electron transfer to the CO_2. On the other hand, comparing the local charges with and without the adsorption, one observes that the charge transferred to the CO_2 strongly depends on the binding mode rather than on the dopant (see Table S3). Upon CO_2 adsorption, the surface C involved in the bonding gets less negatively charged, and CO_2 is highly activated exhibiting a net charge in the -0.76 to -0.98 *e* range. The emerging picture of the adsorption process can be thought as a Lewis acid-base reaction,[40] a feature also reported for the interaction of CO_2 with some oxides.[41] The surface acts as a base transferring charge to the CO_2 acting as an acid.

To further confirm the role played by the charge transfer into CO_2 adsorption on the doped TMCs surfaces, the same analysis has been repeated for other binding modes with a smaller adsorption energy which all display a smaller degree of charge transfer. Thus, a general trend is present where stronger adsorption energies involve concomitant larger charge transfers, a point observed in two-dimensional carbides used in the ammonia synthesis.[42] Lastly, we note that the negatively charged adsorbate would attract other positively charged species such as H^+ with implications in the CO_2 conversion, especially in its electroreduction.

3.6. Work function analysis

The bonding mechanism between doped TiC and CO_2 which we have discussed above and which involves a charge transfer may have observable consequences. In particular, it is likely to affect the surface work function (ϕ), a descriptor for basic-acid characterization of the surfaces.[40] Several studies, both experimental and theoretical, related with CO_2 adsorption in other surfaces such as Ni[43,44] and Co,[45,46] evaluated this property as a chemical activity descriptor although whereas trends along a series are normally trustable[47] it needs to be used with caution.[48]

In the present work only CO_2-free doped TiC(001) surfaces were studied to investigate the predictive nature of such a descriptor regarding dopant effects. Within the present surface slab model, the work function was calculated as the energy difference between the electrostatic potential in the vacuum above the surface, *V*, and the Fermi energy, E_F. This was carried out for the bare undoped surface model, as well as for the doped cases. A dipole correction has been applied in the direction perpendicular to the surface plane to counteract the small surface dipole created by the doping. The results for metal doped TiC (100) surfaces are summarized in Table

3. These results show that low/high work functions tend to favor/disfavor CO_2 adsorption, as expected. However, one must also caution that the relationship between workfunction and CO_2 adsorption is not strong enough so as to conclude a definitive clear direct link between them, which is consistent with previous work.[47,48] Hence, the dopant effects appear to be too local so as to strongly modify the overall surface work function.

3.7. Adsorption/desorption rates

Pressure and temperature are important factors to control the CO_2 adsorption capacity of such metal doped TMCs. The rates of the adsorption and desorption, evaluated through transition state theory, determine whether the CO_2 will be quantitatively stored on the surface or will be desorbed as fast as it will contact on the surface. The adsorption and desorption rate estimates, r_{ads} and r_{des}, respectively, have been obtained following the set up described by Kunkel *et al.*,[10] at the current atmospheric CO_2 partial pressure (40 Pa). Towards this end, the vibrational frequencies of adsorbed CO_2 are required, and calculated with the PBE functionals through diagonalization of the corresponding block of the Hessian matrix with elements obtained from finite displacements of 0.03 Å of the CO_2 molecule analytic gradients. The obtained frequencies allow taking into account the zero point energy (ZPE) in the calculated E_{ads} with values reported in Table 4. Notice that the main effect of the ZPE correction is to reduce the adsorption strength, but it does by up to, at most, 0.03 eV, and therefore can be considered negligible.

Figure 4 reports the CO_2 r_{ads} and r_{des} values for TiC (001) and doped-TiC(001) clearly showing that a small increase on the adsorption energies implies a slight increase of the limit temperature between adsorption and desorption regions. Indeed, for Hf-doped TiC, the adsorption energy is 0.34 eV stronger than for undoped TiC(001), implying an equilibrium temperature between adsorption and desorption of 370 K; this is 135 K higher than the corresponding value for stoichiometric TiC estimated as 235 K.[10] Consequently, Hf-doped TiC would lead to CO_2 capture at higher temperature conditions. For other doping metals, such as W, the temperature decreases, but, in such situations, the previous analysis indicates that CO_2 will preferentially occupy dopant-free surface regions and, as a result, no change in the equilibrium temperature is to be expected.

4. SUMMARY AND CONCLUSIONS

The present DFT based study reports the effects caused by a dopant in the TiC (001) surface on CO_2 capture, storage, and activation. The dopants considered are also early TMs (Hf, Ta, Zr, Nb, W, Cr, Mo, V) placed either at the surface or at the subsurface layer and always replacing a Ti cation. The dopant effect on the geometric and the electronic configurations is found to be highly local. Calculations predict that doping at the outermost surface layer is always preferred over subsurface substitution. The effect of dispersion has been found to equally affect the undoped and doped situations and, therefore, can be considered as a constant. Depending on the dopant, CO_2 adsorption energies can be enhanced, mostly down a group, or reduced, when going along a *d* series.

The results reported in the present work have been obtained for doped TiC but the trends can be easily extrapolated to others TMCs. For instance, according to the observed trends, the Ti-doped VC system would feature an enhanced adsorption energy compared to pure VC. Overall, through surface doping, the CO_2 capture conditions can be tuned, while keeping the activated nature of the chemisorbed molecule.

A meaningful analysis of the CO_2 interaction with such TMCs reveals that the adsorption is driven by the surface CO_2 charge transfer, and that ultimately biased by the surface charge rearrangement/transfer when the doping agent is introduced. We hope that the hereby predicted potential of doped TMCs for CCS and CCU technologies would trigger further experimental work in this field.

ASSOCIATED CONTENT

Supporting Information: Electronic Supplementary Information (ESI) available. See DOI: XXXXXXXXXXX

Table S1. Bader charges on all bare surfaces.

Table S2. Binding modes, adsorption energies with and without van der Waals corrections (vdW), as obtained PBE-D3, as well as geometry parameters, including CO_2 angle, C-C bond distances, *d*(C-C), and CO_2 molecule C-O bond distances, *d*(C-O).

Table S3. Bader charges for all the studied surfaces with adsorbed CO_2.

Figure S1. Top view of the $(3\sqrt{2}\times3\sqrt{2})R45^{o}$ model, the CO_2 was adsorbed both in the shown position but the dopant was moved from Near to Far position.

Figure S2. Top view of the slab model used to represent a higher coverage situation.

NOTES

The authors declare no competing financial interest.

ACKNOWLEDGEMENTS

L. B., J. J. C. and M. N. at Tyndall acknowledge support from the Science Foundation Ireland funded US-Ireland R&D Partnership Program project SusChem grant SFI 14/US/E2915 and from the European Commission funded FP7-NMP project BIOGO, grant number 604296. The SFI/HEA funded Irish Centre for High-end Computing (ICHEC) and SFI funded computing clusters at Tyndall are acknowledged for generous access to computing resources. The work carried out at the *Universitat de Barcelona* has been supported by Spanish *Ministerio de Economía y Competitividad* (MINECO/FEDER) CTQ2015-64618-R grant, *Generalitat de Catalunya* grants 2017SGR13 and XRQTC, and EU H2020 NOMAD project No 676580. F.V. thanks Spanish MINECO for a *Ramón y Cajal* research contract (RYC-2012-10129) and F.I. acknowledges additional support from the 2015 ICREA Academia Award for Excellence in Research.

Table 1. Transition metal cation radii, C-TM distances of the surface and subsurface carbons, doping formation energies, (ΔE_{dop}) and PBE estimated energy differences ($\Delta E_{sub\text{-}surf}$) between surface and subsurface doping sites for TM-TiC(001) surfaces.

Dopant	Radius (Å)	*d*(C-TM) (Å)	ΔE_{dop} (eV)	$\Delta E_{sub\text{-}surf}$ (eV)
Ti^{4+}	0.75	2.17, 2.08	—	—
Cr^{3+}	0.76	2.12, 1.86	3.03	0.64
Hf^{4+}	0.71	2.22, 2.21	-1.19	0.34
Mo^{6+}	0.73	2.16, 1.97	-2.99	0.67
Nb^{5+}	0.58	2.19, 2.07	-1.26	0.39
Ta^{5+}	0.8	2.18, 2.06	-0.07	0.26
V^{5+}	0.68	2.13, 1.93	-2.33	0.26
W^{6+}	0.51	2.15, 1.97	0.71	0.58
Zr^{4+}	0.66	2.24, 2.26	-0.68	0.62

Table 2. Binding modes, adsorption energies, E_{ads}, and corresponding geometrical data, including CO_2 angle, and C-C and C-O bond distances, *d*(C-C) and *d*(C-O), respectively, for the most favorable cases for each transition metal surface dopant at the TiC(001) surface. The remaining adsorption energies and geometries are available at Table S2 of the Supplementary Information.

	CO_2 adsorption				
Dopant	Binding mode	E_{ads} (eV)	CO_2 angle (º)	*d*(C-C) (Å)	*d*(C-O) (Å)
Ti	TopC	-0.61	127.5	1.48	1.29
Cr	TopC-adj	-0.62	128.0	1.49	1.28
Hf	TopC	-0.96	126.0	1.49	1.28,1.30
Mo	TopC-adj	-0.39	128.4	1.50	1.28
Nb	TopC	-0.50	127.0	1.49	1.28,1.29
Ta	TopC	-0.57	127.1	1.49	1.28,1.30
V	TopC-adj	-0.57	127.9	1.49	1.29
W	TopC-adj	-0.31	128.6	1.50	1.28
Zr	TopC	-0.93	125.7	1.50	1.28,1.30

Table 3. Calculated work function (ϕ) and work function variation (Δϕ) of M-TiC doped (001) surfaces.

Dopant	ϕ (eV)	Δϕ (eV)
Ti	3.99	—
Cr	3.99	0.00
Hf	3.93	-0.06
Mo	3.97	-0.02
Nb	3.96	-0.03
Ta	3.95	-0.04
V	3.99	0.00
W	3.96	-0.03
Zr	3.89	-0.10

Table 4. PBE calculated adsorption energies without (E_{ads}) and with ZPE correction (E_{ads}^{ZPE}).

Dopant	Binding Mode	E_{ads} (eV)	E_{ads}^{ZPE} (eV)
Ti	-	-0.61	-0.59
Cr	TopC-adj	-0.62	-0.60
Hf	TopC	-0.96	-0.93
Mo	TopC-adj	-0.39	-0.37
Nb	TopC	-0.50	-0.48
Ta	TopC	-0.57	-0.55
V	TopC-adj	-0.57	-0.54
W	TopC-adj	-0.31	-0.28
Zr	TopC	-0.93	-0.90

Figure 1. PBE optimized structure for the most stable three CO_2 binding modes on the Hf-doped TiC(001) surface slab model. Hf, Ti, C, and O atoms are represented by green, blue, brown, and red spheres, respectively. The carbon from CO_2 is represented by a light brown sphere.

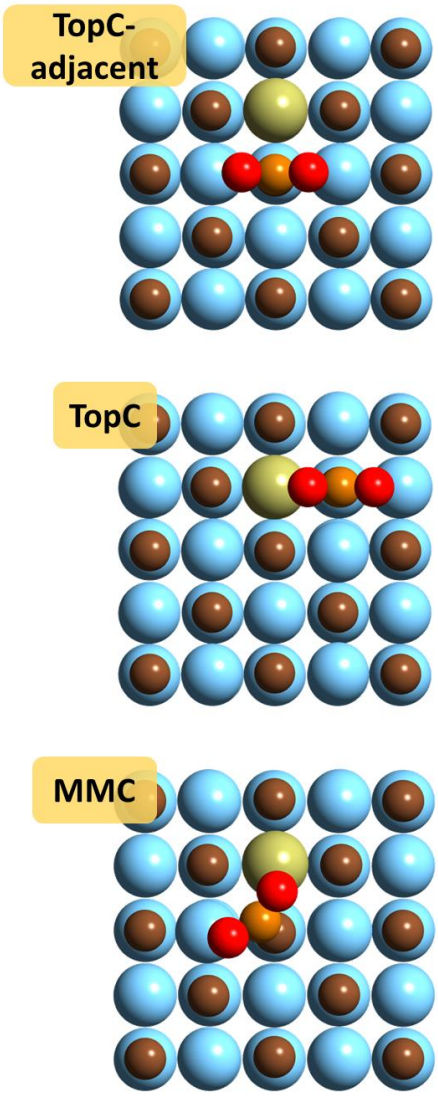

Figure 2. Relaxed atomic structure of CO_2 adsorbed at the Hf-doped TiC (001) surface in TopC binding mode, being the most stable adsorption with an E_{ads} of -0.96 eV. Hf is shown as a pale green sphere. The remaining color code is as on Figure 1.

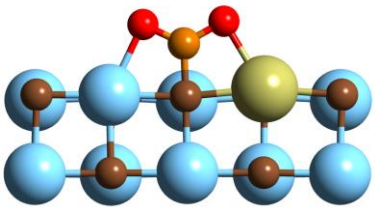

Figure 3. E_{ads} *vs*. Bader charges of the surface doping TM, q^{TM}. A linear fit (R = 0.76) is shown as a red line.

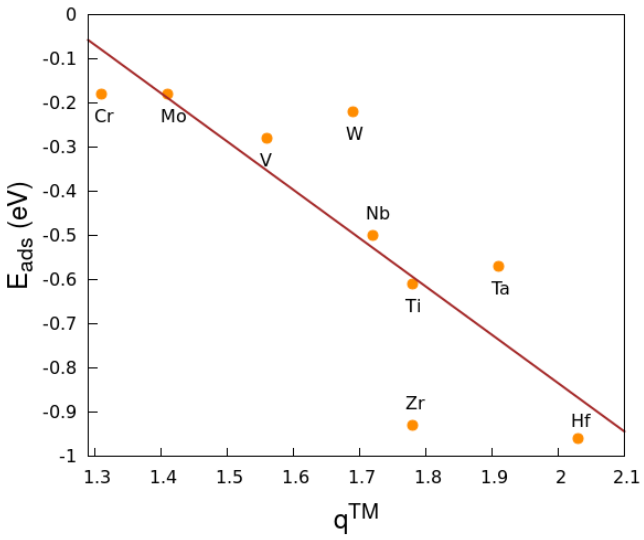

Figure 4. Calculated rates of desorption, r_{des}, and adsorption, r_{ads} of CO_2 on TiC(001) surface at 40 Pa, current partial pressure of atmospheric CO_2. The desorption rates of the undoped and doped surfaces are shown as color-coded lines.

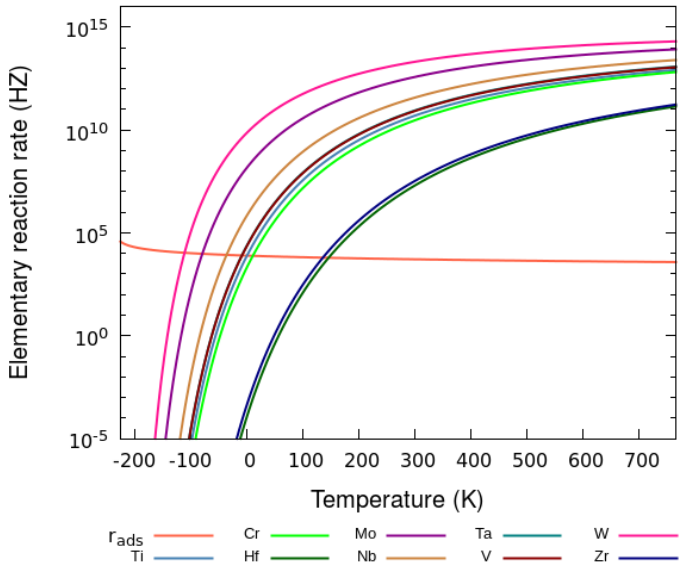

REFERENCES

(1) Filed, C. B.; Barros, V. R.; Jon Dokken, D.; Mach, K. J.; Mastrandrea, M. D.; Bilir, T. E.; Chatterejee, M.; Ebi, K. L. Estrada Y. O.; Genova, R. C.; Girma, B.; et al. *Climate Change 2014: Impacts, Adaptation, and Vulnerability*; **2014**.

(2) Edenhofer, O.; Pichs-Madruga, R.; Sokona, Y.; Minx, J. C.; Farahani, E.; Susanne, K.; Seyboth, K.; Adler, A.; Baum, I.; Brunner, S.; et al. *Climate Change 2014: Mitigation of Climate Change*; **2014**.

(3) Kendon, E.; Roberts, N.; Fowler, H.; Roberts, M.; Chan, S.; Senior, A. C.; Susanne, K.; Seyboth, K.; Adler, A.; Baum, I.; Brunner, S.; Heavier Summer Downpours with Climate Change Revealed by Weather Forecast Resolution Model. *Nature Climate Change.* **2014**, *4*, 570-576.

(4) Cox, P. M.; Betts, R. A.; Jones, C. D,: Spall, S. A,: Totterdell, I. J.; Acceleration of Global Warming due to Carbon-Cycle Feedbacks in a Coupled Climate Model. *Nature.* **2000**, *408*, 184-187.

(5) Doney, S. C.; Fabry, V. J.; Feely, R. A.; Kleypas, J. A.; Ocean Acidification: The other CO_2 Problem. *Annu. Rev. Mar. Sci.* **2009**, 1, 169-192.

(6) UN Doc FCCC/CP/1997/7/Add.1. *Kyoto Protocol to the United Nations Framework Convention on Climate Change* Dec. 10, **1997**; 37 ILM 22 **1998**.

(7) UN Doc FCCC/CP/2009/L.7 *Copenhagen Accord.*18 December **2009**.

(8) UN Doc FCCC/CP/2015/7, Paris Agreement, **2015**, https://unfccc.int/sites/default/files/english_paris_agreement.pdf

(9) International Energy agency (©OECD/IEA). *Global energy and CO_2 status report-2017;* **2018**.

(10) Kunkel, C.; Viñes, F.; Illas, F. Transition Metal Carbides as Novel Materials for CO_2 Capture, Storage, and Activation. *Energy Environ. Sci.* **2016**, *9*, 141–144.

(11) Cheng-Hsiu, Y.; Chihi-Hung, H.; Chung-Sung, T. A Review of CO_2 Capture by Absorption and Adsorption. *Aerosol Air. Qual. Res.* **2016**, *12*, 745-769.

(12) Freund, H.; Roberts, M. W. Surface Chemistry of Carbon Dioxide. *Surf. Sci. Rep.* **1996**, *25*, 225-273.

(13) Espinal, L.; Poster, D. L.; Wong-Ng, W.; Allen, A. J.; Green, M. L. Measurement, Standards, and Data Needs for CO_2 Capture Materials: A Critical Review. *Environ. Sci. Technol.* **2013**, *47*, 11960–11975.

(14) D'Alessandro, D. M.; Smit, B.; Long, J. R. Carbon Dioxide Capture: Prospects for New Materials. *Angew. Chemie - Int. Ed.* **2010**, *49*, 6058–6082.

(15) Markewitz, P.; Kuckshinrichs, W.; Leinter, W.; Linssen, J.; Zapp, P.; Bongartz, R.; Schreiber, A.; Müller, T. E. Worldwide Innovations in the Development of Carbon Capture Technologies and the Utilization of CO_2. *Energy Environ. Sci.* **2012**, *5*, 7281–7305.

(16) Posada-Pérez, S.; Viñes, F.; Rodriguez, J. A.; Illas, F. Fundamentals of Methanol Synthesis on Metal Carbide Based Catalysts: Activation of CO_2 and H_2. *Top. Catal.* **2014**, *58*, 159–173.

(17) Posada-Pérez, S.; Viñes, F.; Ramirez, P. J.; Vidal, A. B.; Rodriguez, J. A.; Illas, F. The Bending Machine: CO_2 Activation and Hydrogenation on δ-MoC(001) and β-

Mo2C(001) Surfaces. *Phys. Chem. Chem. Phys.* **2014**, *16*, 14912–14921.

(18) Li, N.; Chen, X.; Ong, W.-J.: MacFarlene, D. R.; Zhao, X.; Cheetham, A. K.; Sun, C. Understanding of Electrochemical Mechanisms for CO_2 Capture and Conversion into Hydrocarbon Fuels in Transition-Metal Carbides (Mxenes). *ACS Nano* **2017**, *11*, 10825-10833.

(19) Wu, S.; Ho, J. Adsorption, Dissociation, and Hydrogenation of CO_2 on WC (0001) and WC-Co Alloy Surfaces Investigated with Theoretical Calculations. *J. Phys. Chem. C* **2012**, *116*, 13202–13209.

(20) Vidal, A. B.; Feria, L.; Evans, J.; Takahashi, Y.; Liu, P.; Nakamura, K.; Illas, F.Rodriguez, J. A. CO_2 Activation and Methanol Synthesis on Novel Au/TiC and Cu/TiC Catalysts. *J. Phys. Chem. Lett.* **2012**, *3*, 2275–2280.

(21) Porosoff, M. D.; Kattel, S.; Li, W.; Liu, P.; Chen, J. G. Identifying Trends and Descriptors for Selective CO 2 Conversion to CO over Transition Metal Carbides. *Chem. Commun.* **2015**, *51*, 6988–6991.

(22) Yang, H. G.; Sun, C. H.; Qiao, S. Z.; Zou, J.; Liu, G.; Smith, S. C.; Cheng, H. M.; Lu, G. Q. Anatase TiO_2 Single Crystals With a Large Percentage of Reactive Facets. *Nature* **2008,** *453*, 638–641.

(23) Lamiel, O.; Tosoni, S.; Illas. F. Relative Stability of F-Covered TiO_2 Anatase (101) and (001) Surfaces from Periodic DFT Calculations and ab Initio Atomistic Thermodynamics. *J. Phys. Chem. C.* **2014**, *118*, 13667–13673.

(24) Yerskin, I.; Nolan, M. Doping of Ceria Surfaces with Lantanium: a DFT +U Study. *J. Phys. Condens. Matter.* **2010**, *22*, 135004.

(25) Nolan, M. Enhanced Oxygen Vacancy Formation in Ceria (111) and (100) Surfaces Doped with Divalent Cations. *J. Mater. Chem.* **2011**, *21*, 9160–9168.

(26) Liu, Y.; Wen. C.; Guo, Y.; Lu, G.; Wang, Y. Modulated CO Oxidation Activity of M-Doped Ceria (M=Cu, Ti, Zr, and Tb): Role of Pauling Electronegativity of M. *J. Phys. Chem. C* **2010**, *114*, 91889–9897.

(27) Regmi, Y. N.; Leonard, B. M. General Synthesis Method for Bimetallic Carbides of Group VIIIA First Row Transition Metals with Molybdenum and Tungstenum. *Chem. Mater.* **2014**, *26*, 2609-2616.

(28) Kozlov, S. M.; Kovács, G.; Ferrando, R.; Neyman, K. M. How to Determine Accurate Chemical Ordering in Several Nanometer Large Bimetallic Crystallites from Electronic Structure Calculations. *Chem. Sci.* **2015**, *6*, 3868-3880.

(29) Hohenberg, P; Khon, W. Inhomogeneous Electron Gas. *Phys. Rev. B*. **1964**, *136*, 846-871.

(30) Khon, W.; Sham, L. Self-Consistent Equations Including Exchange and Correlaction Effects. *Phys. Rev. A.* **1965**, *140*, 1133-1137.

(31) Perdew, J. P.; Burke, K.; Ernzerhof, M. Generalized Gradient Approximation Made Simple. *Phys. Rev. Lett.* **1996**, *77*, 3865–3868.

(32) Kresse, G.; Hafner, J. Norm-Conserving and Ultrasoft Pseudopotentials for First Row and Transition Elements. *J. Phys. Condens. Matter.* **1994**, 6, 8245-8257.

(33) Kresse, G.; Furthmüller, J. Efficiency of *Ab-initio* Total Energy Calculations for Metals and Semiconductors Using a Plane-Wave Basis Set. *Comput. Mat. Sci.* **1996**, 6, 15-50.

(34) Kresse, G.; Furthmüller, J. Efficient Iterative Schemes for Ab Initio Total-Energy Calculations Using a Plane-Wave Basis Set. *Phys. Rev. B* **1996**, *54*, 11169–11186.

(35) Blöchl, P. E. Projector Augmented-Wave Method. *Phys. Rev. B* **1994**, *50*, 17953–17979.

(36) Kresse, G.; Joubert, D. From Ultrasoft Pseudopotentials to the Projector Augmented-Wave Method. *Phys. Rev. B* **1999**, *59*, 1758–1775.

(37) Monkhorst, H. J.; Pack, J. D. Special Points for Brillouin-Zone Integrations. *Phys. Rev. B* **1976**, *13*, 5188–5192.

(38) Bader, R. F. W. Atoms in Molecules. In *Encyclopedia of Computational Chemistry*; John Wiley & Sons, Ltd: Chichester, UK, 2002.

(39) Grimme, S.; Antony, J.; Ehrlich, S.; Krieg, H. A Consistent and Accurate *Ab Initio* Parametrization of Density Functional Dispersion Correction (DFT-D) for the 94 Elements H-Pu. *J. Chem. Phys.* **2010**, 132, 154104.

(40) Stair, P. C. The Concept of Lewis Acid and Bases Applied to Surfaces. *J. Am. Chem. Soc.* **1982**, *104*, 4044-4052.

(41) Pacchioni, G.; Ricart, J.M.; Illas, F. Ab initio cluster model calculations on the chemisorption of CO2 and SO2 probe molecules on MgO and CaO(100) surfaces. A theoretical measure of oxide basicity. *J. Am. Chem. Soc.* **1994**, *116*, 10152-10158

(42) Miguel-Azofra, L.; Li, N.; MacFarlene, D. R.; Sun, C. Promising Prospects for 2D d^2-d^4 M_3C_2 Transition Metal Carbides (MXenes) in N_2 Capture and Conversion into Ammonia. *Energy Environ. Sci.*, **2016**, *9*, 2545-2549.

(43) Ding, X. Interaction of Carbon Dioxide with Ni (110): A Combined Experimental and Theoretical Study. *Phys. Rev. B* **2007**, *76*, 195425.

(44) Bartos, B.; Freund, H. J.; Kuhlenbeck, H.; Neumann, M.; Lindner, H.; Müller, K. Adsorption and Reaction of CO_2 and CO_2/O CO-Adsorption on Ni(110): Angle Resolved Photoemission (ARUPS) and Electron Energy Loss (HREELS) Studies. *Surf. Sci.* **1987**, *179*, 59–89.

(45) Frerichs, M.; Schweiger, F. X.; Voigts, F.; Rudenkiy, S.; Maus-Friedrichs, W.; Kempter, V. Interaction of O_2, CO and CO_2 with Co Films. *Surf. Interface Anal.* **2005**, *37*, 633–640.

(46) de la Peña O'Shea, V. A.; González, S.; Illas, F.; Fierro, J. L. G. Evidence for Spontaneous CO_2 Activation on Cobalt Surfaces. *Chem. Phys. Lett.* **2008**, *454*, 262–268.

(47) Migani, A.; Illas, F. A systematic study of the structure and bonding of halogens on low index transition metal surfaces. *J. Phys. Chem. B* **2006**, *110*, 11894-11906.

(48) Migani, A.; Sousa, C.; Illas, F. Chemisorption of atomic chlorine on metal surfaces and the interpretation of the induced work function changes. *Surf. Sci.* **2005**, *574*, 297–305 and references therein.

Graphic for TOC